WILEY-VCH

RESEARCH ARTICLE

Solid State Machinery of Multiple Dynamic Elements in a Metal-Organic Framework

Jacopo Perego,[a] Andrea Daolio,[a] Charl X. Bezuidenhout,[a] Sergio Piva,[a] Giacomo Prando,[b] Benjamin Costarella,[b,c] Pietro Carretta,[b] Luciano Marchio',[d] Dominik Kubicki,[e] Piero Sozzani,[a] Silvia Bracco*,[a] and Angiolina Comotti*,[a]

[a] Dr. J. Perego, Dr. A. Daolio, Dr. C.X. Bezuidenhout, Dr. S. Piva, Prof. P. Sozzani, Prof. S. Bracco, Prof. A. Comotti
Department of Materials Science, University of Milano Bicocca, Milan, Italy
E-mail: angiolina.comotti@unimib.it

[b] Dr. G. Prando, Dr. B. Costarella, Prof. P. Carretta
Dipartimento di Fisica, Università degli studi di Pavia, Pavia, Italy.

[c] Dr. B. Costarella
École normale supérieure Paris-Saclay, Gif-sur-Yvette, France.

[d] Prof. L. Marchiò
Dipartimento di Scienze Chimiche, della Vita e della Sostenibilità Ambientale, Università degli studi di Parma, Parma, Italy.

[e] Dr. D. Kubicki
School of Chemistry, University of Birmingham, Birmingham, UK

Supporting information for this article is given via a link at the end of the document.

Abstract: Engineering coordinated rotational motion in porous architectures enables the fabrication of molecular machines in solids. A flexible two-fold interpenetrated pillared Metal-Organic Framework precisely organizes fast mobile elements such as bicyclopentane (BCP) (10^7 Hz regime at 85 K), two distinct pyridyl rotors and *E*-azo group involved in pedal-like motion. Reciprocal sliding of the two sub-networks, switched by chemical stimuli, modulated the sizes of the channels and finally the overall dynamical machinery. Actually, iodine-vapor adsorption drives a dramatic structural rearrangement, displacing the two distinct subnets in a concerted piston-like motion. Unconventionally, BCP mobility increases, exploring ultra-fast dynamics (10^7 Hz) at temperatures as low as 44 K, while the pyridyl rotors diverge into a faster and slower dynamical regime by symmetry lowering. Indeed, one pillar ring gained greater rotary freedom as carried by the azo-group in a crank-like motion. A peculiar behavior was stimulated by pressurized CO_2, which regulates BCP dynamics upon incremental site occupation. The rotary dynamics is intrinsically coupled to the framework flexibility as demonstrated by complementary experimental evidence (multinuclear solid-state NMR down to very low temperatures, synchrotron radiation XRD, gas sorption) and computational modelling, which helps elucidate the highly sophisticated rotor-structure interplay.

Introduction

The study of dynamics in solids is presently a topical issue, since the design and fabrication of smart materials with integrated molecular rotors, motors and switches offers unprecedented opportunities to express innovative properties in response to either chemical or physical stimuli.[1] Relevant examples comprise commutation of light into mechanical work, tunable dielectric and optical properties, the switch of ferroelectricity and on-command gas capture.[2]

Porous materials have been shown as a robust platform providing the necessary free space for dynamics to occur.[3] Self-assembly of appropriate organic modules into Metal-Organic Frameworks (MOFs) provides a versatile strategy to design highly porous 3D crystalline materials with excess free volume wherein limited interference among the dynamogenic moieties can be realized.[4] Among the variety of organic linkers suitable for the assembly of MOFs, fast molecular rotors can be designed and integrated within the backbone of the network considering a few criteria to promote their mobility, including a limited interference among rotors and a low-density scaffold. Additionally, conformational softness to rotation, which is not compatible with extended electronic conjugation and steric hindrance about the mobile elements, is a fundamental feature: these requisites are widely satisfied by aliphatic ligands, which are less common in the realm of MOFs.

Engineering a proper symmetry mismatch of the molecular rotor and the supporting nodes has been a novel principle recently achieved in this family, yielding benchmark rotation with virtually absent energy barrier and frustrated-symmetry rotors.[4a] Specifically, bicyclopentane dicarboxylate ligands (BCP) are optimal candidates as rotors in the frameworks, since they maintain high-frequency motion even in the low temperature limit with the negligeable energy of a few calories per mole.[5] The overall frameworks can be intrinsically endowed with dynamics or flexibility which derive from the geometry of metal nodes or structural phase transitions, showing breathing effects in response to chemical or physical stimuli.[6,7]

Pillared MOFs represent a well-known family which may exhibit reversible dynamic flexibility of the framework when solicited by guest atoms, molecules or simply temperature.[8] Furthermore,

pillared MOFs, being composed by two organized molecular struts, offer the opportunity to design interdigitated networks comprising juxtaposed dynamic elements to fabricate cooperative rotary motion in engineered and elaborated architectures.[5a] Herein, we show the construction of a pillared MOF, named FTR-P2 (belonging to the family of Frustrated Trigonal Rotors), which encompasses multiple co-assembled moving parts, yet integrated into a dynamic machinery, and is governed in turn by the guest-stimulated flexibility of the entire structure. FTR-P2 comprises platforms of BCP dicarboxylate and metal nodes, sustained by azo pyridyl pillars, thus generating four rotating elements: BCP, two distinct pyridyl rings and an azo group. It forms an interpenetrated architecture of two independent networks which undergo reciprocal sliding, switching between two stable states according to the presence or absence of guests which may be loaded in the pores. In the free-pore high symmetry structure, each network is precisely centered in the middle of mutual voids, containing extremely mobile BCP rotors operating at $3.3*10^7$ Hz at 85 K and azo groups with fast mobility of 3.6 kHz at 150 K. Strikingly, bulky guests, such as iodine, dramatically re-structure the framework by reducing symmetry and fuel reciprocal network sliding in a piston-like enlargement of a pore, which promotes BCP rotors to faster mobile regimes of $3.3*10^7$ Hz even down to 44 K. Moreover, the guest-induced piston-like movement induces a circular motion of one pyridyl ring driven by the attached azo group, which behaves as a crank. Contrarily, smaller CO_2 molecules sorbed by the MOF maintain the high symmetry structure and interact with BCP modulating their rotation speed, as observed by in situ synchrotron radiation PXRD of the CO_2-loaded framework up to 10 bar. The dynamics of the molecular rotors, their trajectories and energy barriers were determined by a combined approach, which includes single crystal and synchrotron radiation powder X-ray diffraction, ^{13}C CP MAS down 100 K, ^1H T_1 relaxation times down to 4 K and DFT/MM modelling. Collectively, this work aimed to demonstrate how unconventional integration of rotors (mobile elements) and structural softness can govern a reversible stimulated switch of solid-state molecular motion at surprisingly low temperatures.

Results and Discussion

Pillared FTR-P2 was synthetized by self-assembly two distinct ligands (BCP = bicyclo[1.1.1]pentane-1,3-dicarboxylate and azpy = 4,4′-1,2-diazenediylbispyridine) and Zn ions under solvothermal conditions (75 °C, DMF/MeOH 1:4 mixture) (see Section S2). The synthesis produces dichromic crystals suitable for single crystal X-ray diffraction analysis, which were activated under high vacuum at 120 °C to remove solvent guest-molecules and provide open porosity, while maintaining crystallinity as demonstrated by single crystal and synchrotron source powder XRD patterns (Table S1, Figure S16). The infrared spectrum showed a band assigned to the asymmetric CO_2 stretching vibration of the carboxylate group at 1621 cm^{-1}, which is shifted to lower values of 43 cm^{-1} due to the coordination to the Zn ions with respect to the C=O stretching of the carboxylic acid of BCP ligand (Figure S4). Solution ^1H NMR of digested samples were consistent with a 2:1 ratio between BCP and the bipyridyl ligands (Figure S8). TGA runs displayed sudden weight loss at 300°C, associated to the thermal degradation of BCP and azpy ligands, confirming the stability of the crystals up to those temperatures (Figure S6). Additionally, ^{13}C and ^1H MAS NMR spectra confirmed the purity of the samples and the absence of residual solvent molecules after activation (Figure S17 and S20a).

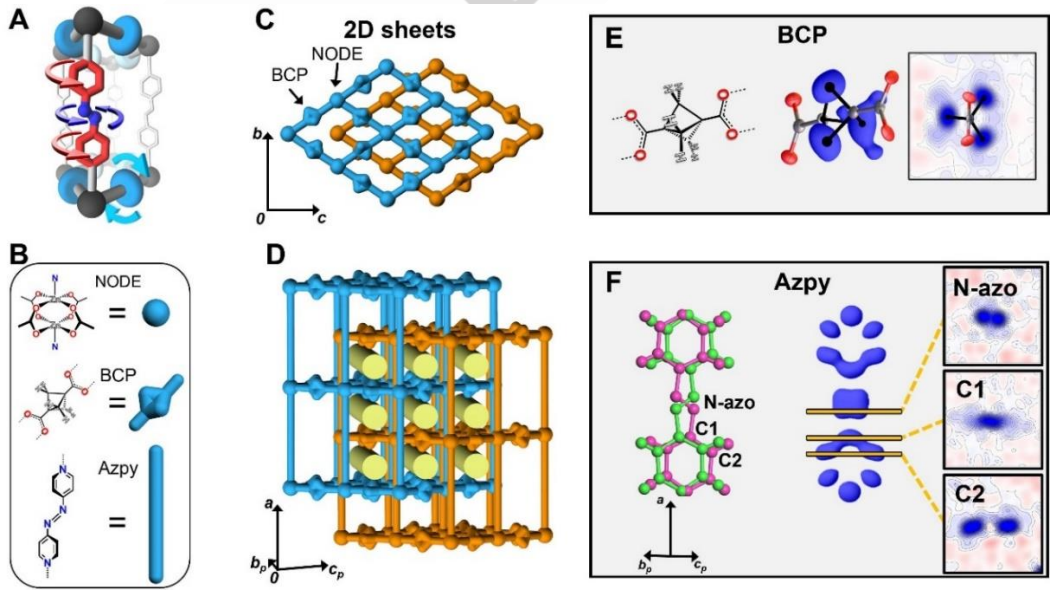

Figure 1. Crystal structure of FTR-P2. A) A single rhombus cube showing the metal node (black sphere) and the connectivity of the ligands, azo group in blue, azpy pyridyl groups in red and the BCP in cyan. B) Zn-paddlewheel node, molecular structures of BCP and azpy linkers. C) 2D layers made by BCP dicarboxylate linkers and Zn nodes forming rhombic shapes. D) The two centre-interpenetrated networks form channel-like cavities shown in yellow. E) The electron density associated with the CH_2 groups of the BCP rotor. F) *Left* - The disorder of the azpy linker with carbons C1 and C2 is highlighted. *Right* – The electron density of azpy linker (from SC-XRD data collected at 200 K) with 2D contours of C1, C2 and the azo nitrogen.

Single Crystal XRD of FTR-P2 revealed a two-fold interpenetrated framework, wherein one network sits in the center of the other (Figure 1). The two ligands, BCP and azpy, play a well-diversified role in the architecture, constituting layers and pillars, respectively. BCP molecules were organized as layers in a rhombohedral motif by coordination to Zn ions in a paddle-wheel fashion, while azobipyridyl pillars sustained the layers. The resulting 2-fold interpenetrated 3D framework has a **pcu** topology[9] and orthorhombic unit-cell, with space group *Cmce* (Figure 1C and 1D). In FTR-P2 structure the pyridyl rings are equivalent by symmetry, and each forms two short hydrogen bonds with the oxygens of the second network nodes, strengthening the layer and pillar 3D architecture (Figure S11)). Both ligands exhibited the signature of dynamic disorder as confirmed by solid-state NMR: first, the three methylene groups of the bicyclopentane ligand showed circularly elongated electron density, which was compatible with a fast rotation on a plane perpendicular to the BCP main molecular axis (Figure 1E). Diffuse electron density was also manifested in pillar azo-groups, associated with pyridyl rings swinging on a common plane, indicative of a pedal-like motion (Figure 1F).[10] The interpenetrated framework displays 1D corrugated channels running parallel to the *b*-axes, ca. 10% of the crystal volume, with cross-sections ranging from 6.0 x 2.9 $Å^2$ to 3.8 x 3.8 $Å^2$. No residual electron density was observed inside the channels. The open porosity of the framework was demonstrated by CO_2 adsorption isotherms at 195 K up to 1 bar (Figure S9). FTR-P2 displayed a maximum adsorbed amount of about 3.2 mmol/g (ca. 8 molecules per unit cell). Interestingly, FTR-P2 adsorbs neither N_2 and Ar at 77 K nor N_2 at 298 K, due the molecular sieving effects of the small pores (Figure S10). As a consequence of the above-mentioned pore selectivity of activated FTR-P2 with small and selective pores, the structure should prevent the bulky molecular iodine diffusing-in. However, contrary to the expectations, the crystals visibly absorb I_2 without fracturing, thus yielding crystals suitable for SC-XRD. I_2 inclusion, about 4 molecules per unit cell as quantified from TGA (Figure S7), enables a remarkable channel expansion, driven by the displacement of the interpenetrated networks, as revealed by the SC-XRD of the black I_2-loaded crystals (Figure 2A). The reciprocal sliding of the two networks along the pillar direction of 2.45 Å thereby transforms the centered interpenetrated architecture to a new off-centered one, expanding one channel while virtually closing the adjacent one, resembling a piston movement which pushes layers apart by I_2 action (Figure 2A). The structural resolution of the FTR-P2-I_2 and the localization of I_2 was obtained by combining *ab initio* calculations with fitting of experimental SC-XRD data (Figure S14 and S15). The I_2 molecules can be entirely removed by thermal treatment at 180°C, as directly followed by thermal gravimetry (Figure S21). The empty structure was fully restored as shown by PXRD pattern and ^{13}C CP MAS NMR, demonstrating the reversibility of the piston movement and the cyclability of the phenomenon (Figure S24, S25 and S27).

Following iodine insertion, the β-angle changes from 90° to 97°, thereby changing the crystal system from orthorhombic (*Cmce*) to monoclinic (*C2/m*, Figure 2A). Unlike the empty structure, the coordination of the two BCP carboxylate moieties with the Zn ions and the main BCP axis are aligned (Figure S12). In this off-centred phase, the two rings of the pillaring ligand are no longer equivalent: one ring (A) is exposed to the channels while the other (B) sits in the plane of the 2D layers. Ring B is placed at the centre of the rhombus and is close to the metal nodes, forming multiple C-H···O hydrogen bonds with the carboxylate oxygens, which pin its position inside the 2D layer (Figure 2D). In contrast, ring A gains freedom and explores multiple configurations reflected in four electron density maxima associated with carbons C2 and C3 distributed along an arch (Figure 2D). The Na of azo group, on which the ring A is pivoted, is off-plane with respect to ring B and shows electron density delocalized on two distinct positions separated by 1.2 Å. The motion of the azo group between these two sites consequently induces a crank-like motion of the pivoting ring A, as modelled by MM calculations (Figure S65).

Interestingly, the I_2 molecules confined inside the channels are localized in two distinct crystallographic environments, denoted I_2-A and I_2-B (Figure 2B) and disordered over multiple equivalent positions in each environment (Figure S15). The axes of I_2-B molecules are in the most confining part of the channels and approximately are mainly aligned along the *c* axis (slightly tilted towards *a* axis) whilst I_2-A molecules lie along the *b* axis. Both I_2 arrangements form intermolecular interactions with the aromatic ring A (Figure S15B). Out of four I_2 molecules per unit cell, two sit in I_2-A site and two in I_2-B site, in agreement with thermogravimetry and PXRD pattern (Figure S21 and S25, respectively).

Surprisingly, even with I_2 molecules occupying the framework channels, the electron density of the BCP ligand is more spread out than that of the empty structure, describing a toroidal shape. This diffuse density indicates a major disorder of the rotor, thus suggesting increased dynamics, instead of the commonly described hindering action of guest molecules.[11]

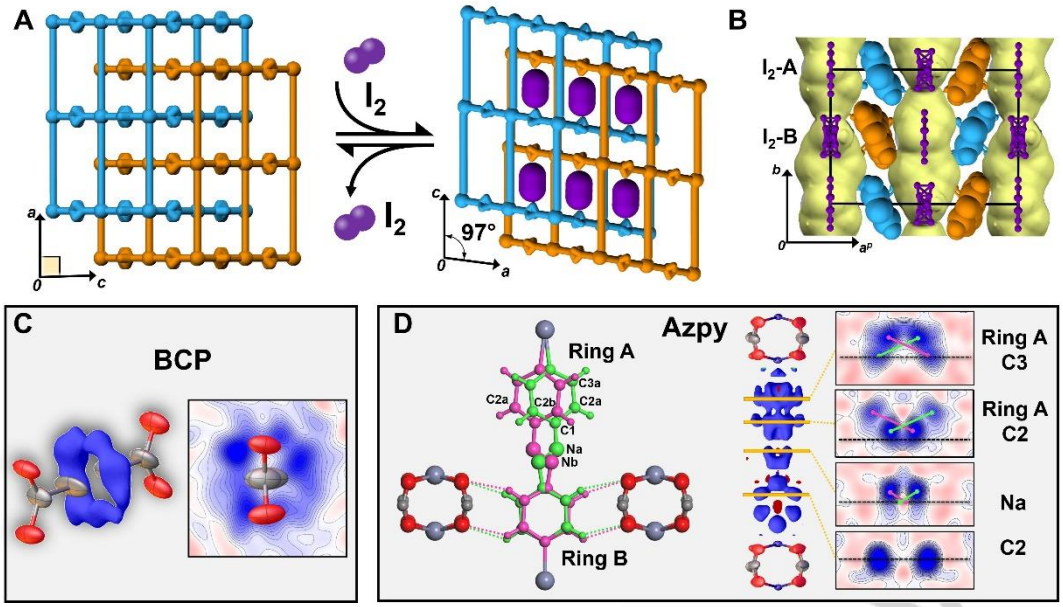

Figure 2. A) The reversible structural transformation of FTR-P2 upon inclusion of I_2. As viewed along the *b* axis with the γ-angle highlighted. B) FTR-P2-I_2 structure as viewed along the *c*-axis, highlighting the channels (light yellow) and the highly disordered I_2 molecules (iodine: violet). C) Diffused electron density with a toroidal shape about the main BCP axis shows increased BCP rotor dynamics. D) *Left* - The disorder of the azpy linker with atoms C1 and C2A, C2B, C3A, Na and Nb for Ring A highlighted. Ring B is shown to form interactions with the carboxylate oxygens. *Right* – The electron density of azpy linker (from SC-XRD data collected at 200 K) with 2D contours of C2 Ring B and C2 and C3 of Ring A and the azo nitrogen Na.

High resolution ^{13}C MAS NMR is a method of choice to understand the environment explored by each carbon atom within the observation time-scale. Variable temperature experiments under magic angle spinning and cross polarization were performed on FTR-P2 and FTR-P2-I_2 from room temperature to 100 K at ^{13}C NMR frequencies of 75 MHz and 100 MHz (Figure 3 and Figure S29 and S31). The first prominent observation is a single methylene signal for BCP rotors, detected at any acquisition temperature for both the samples, indicating the fast motional exchange about its rotational axis.

Regarding the pillars, the high symmetry of the unit cell of FTR-P2 entails the equivalence of the homologous carbons in the two pillar rings. Signal multiplicity is significantly modulated by temperature: indeed, on lowering the temperature, we observe a broadening of the C2 resonance and two distinct signals appearing at about 136 K, suggesting two non-equivalent environments for C2 carbons that are affected by the dihedral angle θ = C2-C1-N=N (Figure 3B). The chemical shifts of C2 carbons depend on their arrangement with respect to the azo group (syn or anti). The C2 in the syn conformation (θ ≈ 11°) is shifted to higher frequencies compared to the C2 carbon in the anti conformation (θ ≈ 169°).[12] Above 150 K a coalescence signal due to the averaging of C2 chemical shifts is observed unveiling fast pedal-like motion of the azo-group with k_{exch} > 3630 Hz. This finding agrees with the diffused electron density of the nitrogens in the SC-XRD (Figure 1F). FTR-P2 scan computed with Molecular Mechanics for a 360° rotation of the azo moiety confirmed the occurrence of pedal-like motion (Figure S60).[10]. The high symmetry of the crystal structure at room temperature is confirmed by the presence of only two signals in the ^{15}N MAS NMR spectra, which are assigned to the pyridyl nitrogens and azo group (Figure S32). Additionally, the observation of a marked motional broadening[12] of the ^{13}C MAS NMR signals in the 270 - 280 K range (Figure S30) reveals the fast reorientation of pyridyl rings in the 10^5 Hz regime with respect to the framework, consistent with the energy barrier estimated by theoretical calculations (Figure S61).

For FTR-P2-I_2, a completely different behavior is observed for the azpy ligands. The reciprocal sliding of the two interpenetrated networks from FTR-P2 by I_2 absoption, as determined by SC-XRD, is mirrored in the dramatic changes of ^{13}C MAS NMR spectra, owing to the distinct environments of each aromatic ring. Additionally, on going from the empty to the I_2-containing framework, the piston-like sliding imprints its remarkable effect on the dynamics of each aromatic ring. The symmetry change is apparent in the splittings of all three signals of the azpy pillar (as also confirmed by ^{15}N MAS NMR, see Figure S32). Focussing on the C2 carbon signal, a complex modulation with temperature is observed: we can discriminate two families of signals pertaining to the two rings (Figure 3C red and blue colors).

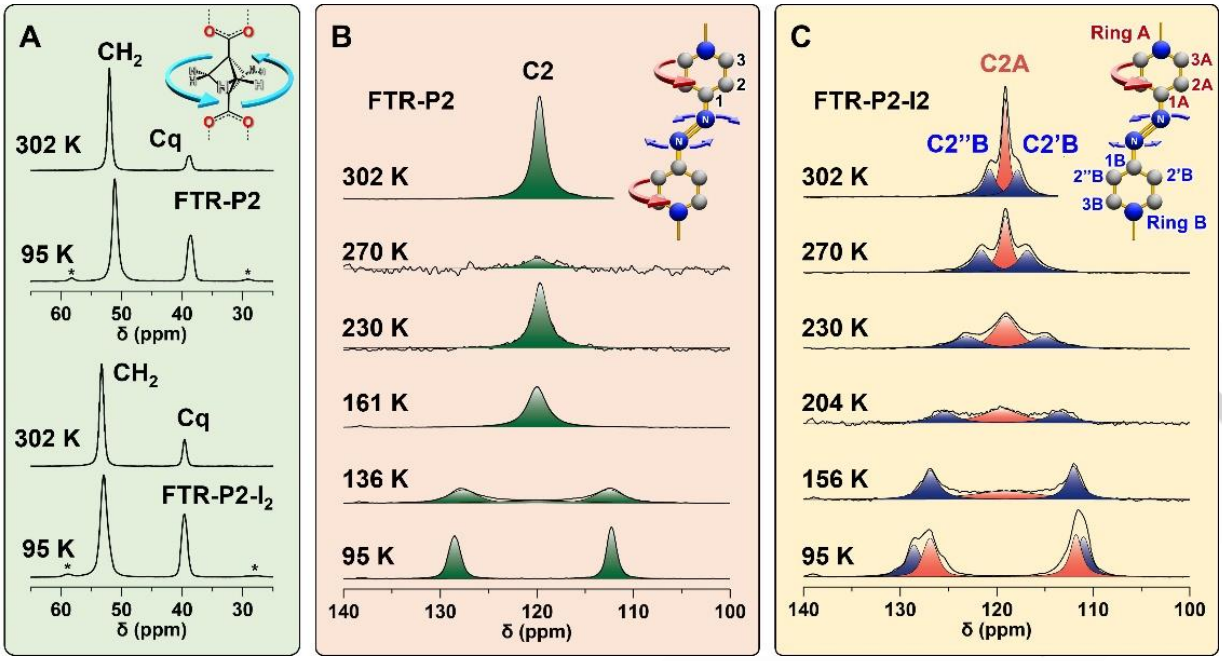

Figure 3. ^{13}C {^{1}H} CP MAS spectra collected at variable temperatures, 7.04 T, 8.0 kHz and a contact time of 2 ms for 302-230 K temperature range, (12.5 kHz for 302 K), 9.40 T, 10 kHz and a contact time of 6 ms for lower temperatures. A) BCP CH_2 and Cq signals of FTR-P2 (*top*) and FTR-P2-I_2 (*bottom*), B) Azpy C2 signal of FTR-P2, and C) Azpy C2 signals of FTR-P2-I_2. All the spectra of B) and C) were scaled to match the intensity of the BCP carboxylate peaks. Full spectra are reported in Figures S29 and S31.

A couple of resonances (Figure 3C: marked by red) undergoes coalescence on increasing the temperature from 95 K to 150 K. A different behavior was observed for the second couple of signals (Figure 3C: marked by blue), whose chemical shift difference decreases progressively on increasing the temperature in the 95-302 K range. Indeed, molecular mechanics and PW-DFT calculations predict a asymetric potential for the reorientation of the azo group by 180°, with an energy difference of 2 kcal/mol (Figure S65).[13] On the contrary in the empty system, the azo group reorients between two energetically and structurally equivalent sites. At 95 K, carbon C2'B is substantially in the *syn* conformation with respect to Na (θ = Na-Nb-C1-C2'B). However, the azo group reorientation upon increasing temperature leads carbon C2'B to explore *anti* conformation according to Boltzmann distribution (Figure S67). These changes in population distribution for C2'B result in the observed peak shifting to higher frequencies from δ = 111.7 to 117.8 ppm upon increasing temperature (Figure 3C: blue signals). The same mechanism applies to carbon C2''B but in reverse, moving the peak to lower frequencies upon increasing temperature (from δ = 127.0 to 120.7 ppm). This mechanism of motion is ascribed to the azo group since ring B is embedded in the 2D layer, and its reorientation requires a high energy barrier, as shown by long ^{13}C T_1 relaxation times in the solid regime (Table S13). On the contrary, the mechanism of ring A reorientation is more complex and involves both the azo group and the pyridyl ring with reorientation phenomena of comparable activation energies, yielding two equivalent arrangements for the C2'A and C2"A carbons and thus the coalescence of their signals (Figure 3C: red set of signals).

The dynamics of BCP molecular rotors was demonstrated by spin-lattice relaxation times (T_1) as a function of temperature. Notably, ^{13}C NMR spin-lattice relaxation times of BCP in both FTR-P2 and FTR-P2-I_2 from room temperature to 200 K evidence that the relaxation behavior happens in the extreme narrowing regime ($\omega_0\tau_c$ << 1), typical of liquids. This result shows the BCP moiety is highly dynamic with rotational frequencies higher than the observation frequencies of 75 MHz and 100 MHz, corresponding to the ^{13}C Larmor frequencies (Figure 4). Interestingly, the presence of I_2 in the channels did not hamper the dynamics of BCP rotors but lowered the energy barrier slightly by 0.3 kcal/mol compared to the empty framework (Figure 4A-inset).

An in-depth study of the motional behavior was provided by ^{1}H T_1 relaxation times of both the samples collected over a wide temperature range down to 4 K (Figure 4A). The relaxation rate profile of FTR-P2 fitted by Kubo-Tomita equation[14] is in full agreement with a progressive slowdown of dynamics on decreasing temperature, still exploring the high-frequency regimes of about 10^7 Hz (33.8 MHz) at 85 K and $7*10^5$ Hz at 45 K. The activation energy for rotation was 1.2 kcal/mol and the attempt frequencies of about $4.7*10^{11}$ Hz (τ_0= $2.1*10^{-12}$ s) for BCP, consistent with independent rotors of rotating inertial masses of 42 (BCP, theoretical τ_0= $2.45*10^{-12}$ s).[15] The same energy barrier was also determined by ^{13}C T_1 relaxation times (Figure S36). The NMR measurements performed even with the application of different thermal ramps were fully reproducible, showing the robustness of the material. 2D DFT potential energy scans, using M062X/6-311+G(d) level of theory, were used to calculate the energy for rotation of BCP

rotors as arranged in the crystal structure (rotors R1 and R2). Two lowest energy rotation pathways could be extracted, which also pass through the global minimum of the system, thus proving that single rotor rotations are effective even in the porous framework (Figure 4C). Additionally, the calculated energy barriers are 1.03 and 1.26 kcal/mol, which are congruent with the experimental value of 1.2 kcal/mol (Figure 4B).

After the iodine-induced piston-like sliding of the framework, the profile of the ^{1}H NMR relaxation rates showed a distinct broadening. The overall dependence of the relaxation rate on the temperature is consistent with the sum of multiple Kubo-Tomita contributions whose maxima are markedly shifted to lower temperatures centered at 44, 61, 74 and 87 K, indicating the augmented mobility with lower energy barriers of 0.6, 0.8, 1.0 and 1.2 kcal/mol (the attempt frequency = $3*10^{12}$ s). For the I_2-loaded structure (Figure 4A), 2D DFT potential energy scans were performed considering four unique rotors (R1, R2, R3 and R4) and their nearest iodine molecules as positioned in the FTR-P2-I_2 crystal structure (Figure 4D). The lowest energy pathways, yielded by the 2D energy scans, unveiled the occurrence of single rotor rotation even in the presence of the bulky I_2 molecules in the pores. Specifically, two rotational pathways for R1 with barriers of 0.6 and 0.87 kcal/mol (P1 and P2) and two rotational pathways for R2 of 1.2 and 1.4 kcal/mol (P3 and P4) were estimated and agree with the experimental barriers measured by ^{1}H and ^{13}C T_1 NMR. The average energy of R1 rotations is 0.4 kcal/mol lower with respect to R2 due to the much weaker rotor-iodine interactions of R1 (0.36 kcal/mol maximum) compared to R2 (1.0 kcal/mol maximum) (Figure 4E). The stronger interactions between R3/R4 and the iodine molecules increase their rotational barriers to above 2 kcal/mol, with average energies more than 2 kcal/mol higher than R1. Thus, the guest intervention did not entail rotor hampering, as it would conventionally be predicted because of the guest steric encumbrance and intermolecular interactions; instead, iodine molecules pushed the network sliding, liberating the dynamics of both BCP and the channel-exposed ring A rotor.

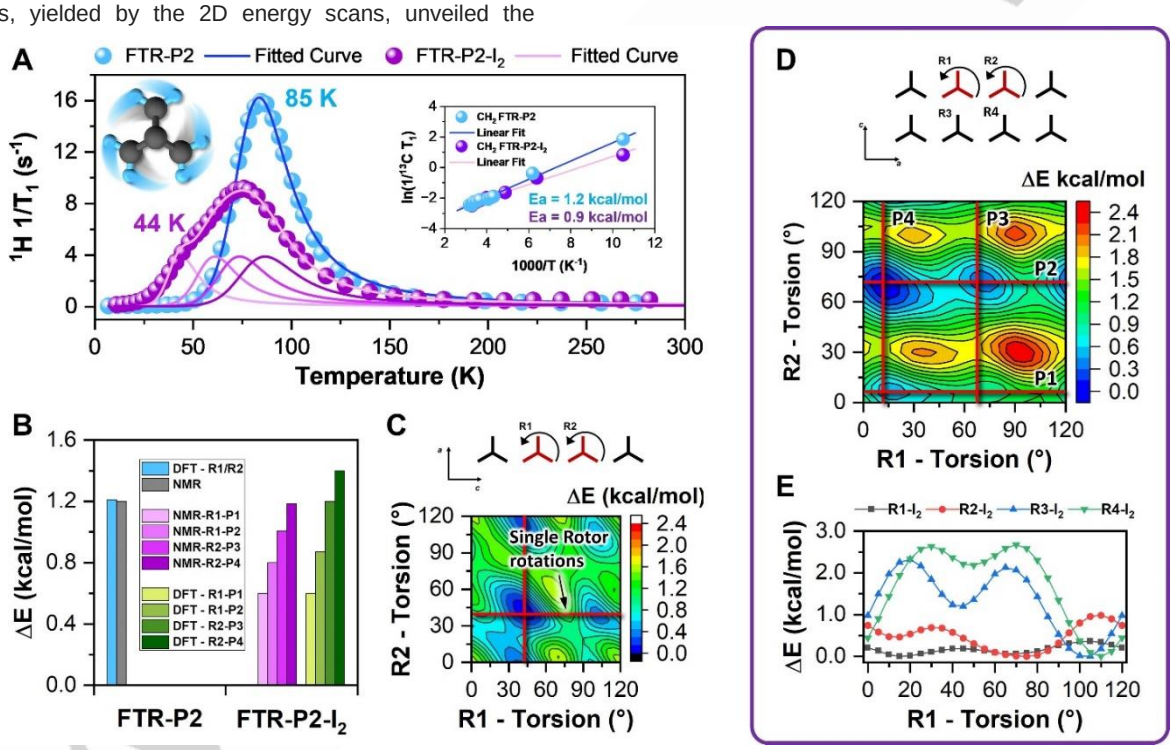

Figure 4. A) ^{1}H relaxation rates as a function of temperature for FTR-P2 (blue circles) and FTR-P2-I_2 (purple circles). The fitted Kubo-Tomita functions are shown in solid lines. In the inset, variable temperature ^{13}C T_1 relaxation times of CH_2 collected at 75 and 100 MHz for both FTR-P2 (blue circles) and FTR-P2-I_2 (purple circles). B) The bar chart shows the comparison between the NMR determined rotational barriers and the DFT computed barriers (for FTR-P2: grey and blue bar, respectively). In the case of the FTR-P2-I_2, multiple rotational barriers were found, two for R1 and two for R2. C) FTR-P2 2D scans calculated by DFT. *Top* – computational model and schematic representation of the 2D scan computational model. *Bottom* - The potential energy map for the 2-D scan of rotors R1 and R2 is shown. The red lines indicate the lowest energy rotations passing through the minima of the system. D) FTR-P2-I_2 2D scans calculated by DFT. *Top* - Schematic representation of the 2D scan computational model, the interacting azpy pillars and Iodine molecules have been omitted for clarity. *Bottom* - The potential energy map for the 2-D scan of rotors R1 and R2 is shown. The red lines (P1, P2, P3 and P4) indicate the lowest energy rotations passing through the minima of the system. E) Potential energy scans for the interaction between the unique rotors and the iodine molecules.

The empty FTR-P2 adsorbs efficiently CO_2 between 253 K - 298 K up to 1 bar (Figure 5), and thus, we explored the dynamics of the framework in response to CO_2 as an alternative guest. An enthalpy of adsorption at low coverage of

30 kJ/mol was estimated by microcalorimetry coupled with adsorption analyzer for the simultaneous acquisition of gas adsorption enthalpy and gas loading (Figure S78). Contrarily, nitrogen could not enter the small pores of the structure: the very distinct sorption behavior of CO_2 *vs* N_2 suggests that FTR-P2 is suitable for gas separation. Under operative conditions of gas-mixture streams with 15% and 5% CO_2 over N_2, at 298 K, CO_2 was completely separated from the mixture whilst N_2 passed through the column and was collected with a purity of more than 99% for 5.0 min g^{-1} and 6.4 min g^{-1}, respectively, as assessed by breakthrough adsorption experiments (Figure S82).

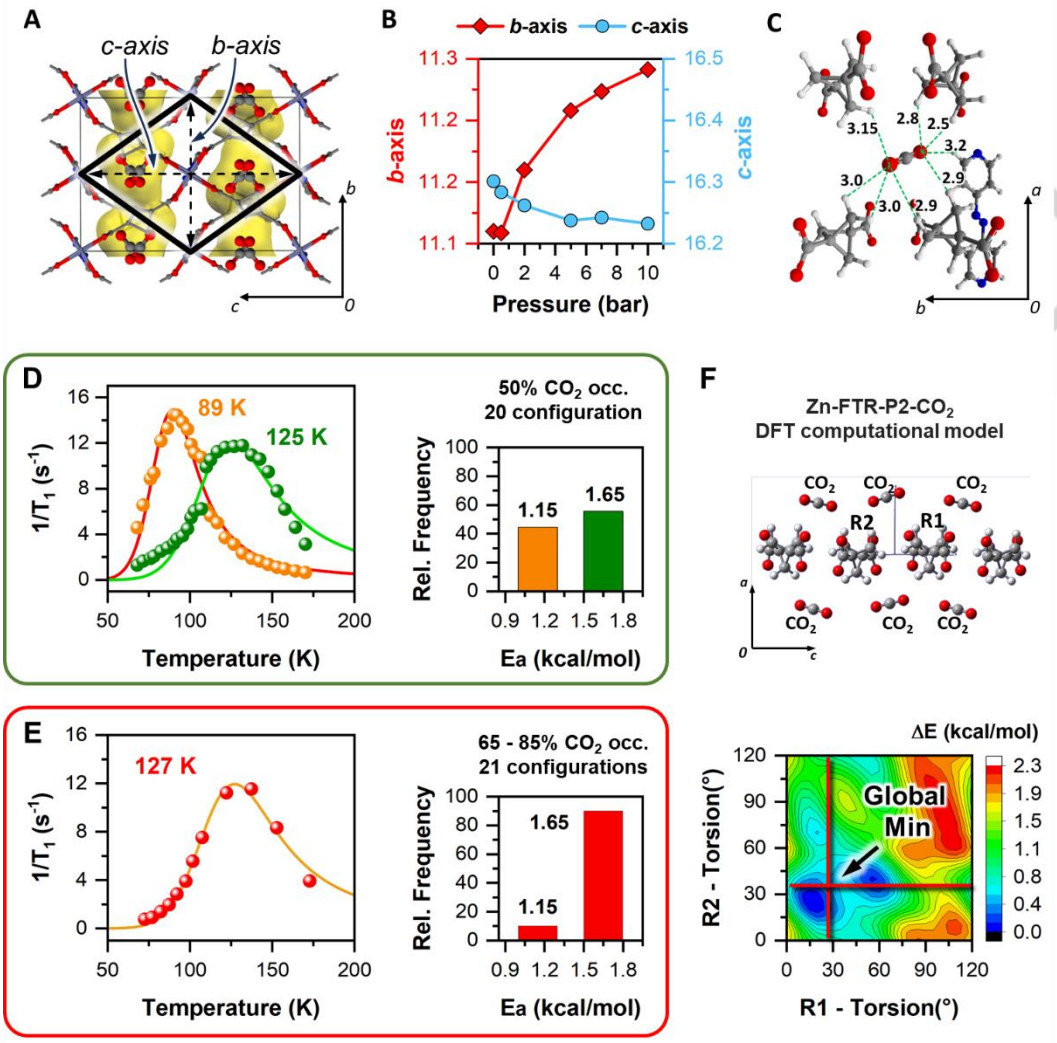

Figure 5. A) The structure for FTR-P2-CO_2-10bar obtained by Rietveld refinement against data collected using synchrotron radiation under 10 bars of CO_2 gas and room temperature (293 K) viewed down (1 0 0) with the channels shown in yellow and the CO_2 molecules in ball-and-stick representation. The rhombus of the carboxylate network is shown with the diagonal indicated using double-sided arrows as well as their corresponding cell axes. B) The *b*- and *c*-axes (the diagonals of the rhombus) plotted versus CO_2 gas pressure. C) The interactions between the CO_2 molecule and MOF as shown in green dashed lines. The interactions are mostly between CO_2 and the hydrogens of the BCP CH_2 groups. The distances are indicated in Å. D) ^1H T_1 NMR relaxation times of FTR-P2-CO_2 collected at variable temperature and frequency of 33.77 MHz. *Top* – 50% loading of CO_2 in FTR-P2. *Bottom* – Fully loaded CO_2 FTR-P2. The data were fitted by Kubo-Tomita function. E) The histogram relative frequency plots for the BCP rotational barriers calculated by DFT considering the possible configurations of CO_2 over the various sites. *Top* – 50% CO_2 loading (the two relaxation rates are quantified from the double-exponential shape of the recovery law). *Bottom* – 65 – 85% CO_2 occupancy. The histograms are centred around two energy barrier values, 1.15 and 1.65 kcal/mol, with almost equal distribution up to 50% CO_2 and mainly distributed on 1.65 kcal/mol for the 65 – 85% CO_2 loading. F) FTR-P2-CO_2 2D scans and relative activation energies. *Top* – the view along (0 1 0) to highlight the arrangement of the CO_2 molecules with respect to the BCP rotors. *Bottom* – The potential energy map for the DFT 2-D scan of rotors R1 and R2 considering 50% CO_2 is shown as an example. The red line shows the lowest energy rotations, single rotor rotations, passing through the global minimum of the system. Energy barriers were extracted for different CO_2 occupancies and configurations. All these rotational barriers were then analyzed statistically using a histogram with a bin width of 0.4 kcal/mol.

CO_2 molecules, with their small size (kinetic diameter of 3.3 Å) and its quadrupolar nature, could enter the pores of the empty structure and did not slide the networks with respect to each other (as for I_2 capture), which was demonstrated by

synchrotron radiation powder XRD under CO_2 gas pressure up to 10 bar at room temperature (Figure S85 and Table S31). The crystal structure was refined with a high symmetry *Cmca* space group. The maximum CO_2 occupancy at 10 bars, as estimated by Rietveld refinement, is of 6 MPU, corresponding to 75% of the maximum loading of 8 MPU determined by the CO_2 adsorption isotherm at 195 K. The crystal structures show that the *b*-axis increases upon increased CO_2 loading. The stretching of the *b*-axis slightly moves the sorption sites apart along the channel direction for optimal CO_2-CO_2 interactions and inclusion of CO_2 into the pores. The CO_2 molecules are tilted with respect to the channel direction and ca. parallel to the *bc* plane, thus avoiding repulsion between the oxygen atoms of vicinal CO_2 molecules. The CO_2 molecules are off-centered with respect to the channel axis and disordered over two symmetry-equivalent positions. Importantly, CO_2 molecules install effective C-H···O interactions between BCP molecular rotors and CO_2 oxygens.

The highly efficient CO_2 capture reduced mobility as shown by the ^1H $1/T_1$ maximum of Kubo-Tomita curve which is shifted to higher temperatures for BCP molecular rotors compared to the empty structure. The FTR-P2 sample fully loaded with CO_2 showed a peak maximum shifted up to 127 K, evidence of CO_2 interactions with the BCP rotors. Thus, the energy barrier increased from 1.1 to 1.5 kcal/mol while the attempt frequency $1.5*10^{11}$ Hz ($\tau_0 = 6.5*10^{-12}$ s) fell in the typical single rotor rotation range.

DFT calculations for estimating the BCP rotational barrier upon increasing CO_2 loading in FTR-P2 resulted in considering several CO_2 configurations. The CO_2 configurations about the rotors generate two main dynamics associated with the two unique R1 and R2 rotors (Figure 5F) with rotational barriers concentrated around two values, 1.15 and 1.65 kcal/mol. Loadings up to 50% produce an almost equal distribution for the two rotational barriers, resulting in a recovery of the nuclear magnetization with markedly double-exponential character (Figure S2). In comparison, for loading between 65% and 85%, the 1.65 kcal/mol rotational barrier prevails, in agreement with the energy barriers measured by the simulation of ^1H T_1 relaxation times. These results show a strong correlation between the multiple intermolecular interactions between the CO_2 oxygen atoms and the BCP hydrogen atoms and the dynamics of the BCP rotor.

Conclusion

The design and fabrication of a dynamic machinery that comprises several mobile elements of diverse nature and symmetry were accomplished successfully in a pillared Metal Organic Framework. Multiple molecular rotating elements, such as bicyclopentane, pyridyl, and trans azo-groups, were integrated into a flexible framework, which guides an intriguing concerted dynamics of the individual components. As the result of the open porosity, both structure and rotary motion were fine-tuned and even enhanced, in response to stimuli, as diffused CO_2 or I_2 vapors. Indeed, the dynamic MOF undergoes a piston-like displacement of the framework, propelled by the guest absorption.

These fully-dynamical solids promote intrinsic motility at low temperatures where the molecular motions of most materials are frozen. The BCP, pyridyl and azo groups are known to manifest their mobility individually, however, integration in a common tunable framework generates additional diversified local environments, thus exploring unprecedented motional mechanisms and interactions.

This example highlights the degree of control over dynamics and symmetry obtainable by the design of "rotors-in-a-scaffold" combined with a crystal architecture endowed with reciprocally sliding networks. The soft, low-activation-energy landscape of these prototypal materials stimulates a dynamical yet structurally stable playground for enabling sophisticated responsive machines in solids. This exquisite interplay of framework and local dynamics will be helpful for the construction of switchable ferroelectric materials, switches and actuators. Moreover, the reversible uptake/release of I_2 molecules promises access to applications of capture of radioactive I_2 and material recyclability.

Acknowledgements

Ministry of University (MUR) for PRIN 2020EZ8EPB (SHERPA) and Lombardy Region for ''Enhancing Photosynthesis'' grant (2021-2023) are acknowledged for the financial support. The authors also acknowledge the Horizon Europe project PANACEA "Pan-European Solid-State NMR Infrastructure for Chemistry-Enabling Access", (H2020, Grant N.101008500_Göteborg) and Arthur Pinon for technical support. We would like to thank the European Synchrotron Radiation Facility (ESRF) in Grenoble (France) for the access to the ID22 beamline (Project HC-5193) and Giorgia Confalonieri for technical support. D.J.K. acknowledges the ERC-selected PhotoPeroNMR project funded by UKRI Horizon Europe guarantee (EP/Y01376X/1).

Supporting Information

The raw NMR data are available on Zenodo [link to be added at proof stage].

Keywords: Crystal Engineering • Metal Organic Frameworks • Molecular Dynamics • Molecular Rotor • Solid State NMR

[1] a) S. Krause, B. L. Feringa, Towards Artificial Molecular Factories from Framework-embedded Molecular Machines. *Nat. Rev. Chem.* **2020**, *4*, 550-562. b) P. Martinez-Bulit, A. J. Stirk, S. J. Loeb, Rotors, Motors, and Machines Inside Metal–Organic Frameworks. *Trends in Chem.* **2019**, *1*, 588-600. c) D. Dattler, G. Fuks, J. Heiser, E. Moulin, A. Perrot, X. Yao, N. Giuseppone, Design of Collective Motions from Synthetic Molecular Switches, Rotors, and Motors. *Chem. Rev.* **2020**, *120*, 310-433. d) L. Feng, R. D. Astumian, J. Fraser Stoddart, Controlling dynamics in extended molecular frameworks. *Nat. Rev. Chem.* **2022**, *6*, 705-725.

[2] a) N. Koumura, R. W. J. Zijlstra, R. A. van Delden, N. Harada, B. L. Feringa, Light-driven monodirectional molecular rotor *Nature* **1999**, *401*, 152–155. b) Q. Li, G. Fuks, E. Moulin, M. Maaloum, M. Rawiso, I. Kulic, J. T. Foy, N. Giuseppone, Macroscopic contraction of a gel induced by the integrated motion of light-driven molecular motors. *Nat. Nanotech.* **2015**, *10*,161-165. c) C. Lemouchi, K. Iliopoulos, L. Zorina, S. Simonov, P. Wzietek, T. Cauchy, A. Rodríguez-Fortea, E. Canadell, J. Kaleta, J. Michl, D. Gindre, M. Chrysos, P. Batail, Crystalline Arrays of Pairs of Molecular Rotors: Correlated Motion, Rotational Barriers, and Space-Inversion Symmetry Breaking Due to Conformational Mutations. *J. Am. Chem. Soc.* **2013**, *135*, 9366-9376. d) S. Bracco, M. Beretta, A. Cattaneo, A. Comotti, A. Falqui, K. Zhao, C. Rogers, P. Sozzani, Dipolar Rotors Orderly Aligned in Mesoporous Fluorinated Organosilica Architectures. *Angew. Chem. Int. Ed.* **2015**, *54*, 4773-4777. e) P. Naumov, D. P. Karothu, E. Ahmed, L. Catalano, P. Commins, J. M. Halabi, M. B. Al-Handawi, L. Li, The Rise of the Dynamic Crystals. *J. Am. Chem. Soc.* **2020**, *142*, 13256-13272. f) F. Castiglioni, W. Danowski, J. Perego, F. K.-C. King-Chi Leung, P. Sozzani, S. Bracco, S. J. Wezenberg, A. Comotti, B. L. Feringa, Modulation of porosity in a solid material enabled by bulk photoisomerization of an overcrowded Alkene. *Nat. Chem.* **2020**, *12*, 595-602.

[3] a) H. Deng, M. A. Olson, J. F. Stoddart, O. M. Yaghi, Robust Dynamics. *Nat. Chem.* **2010**, 2, 439-443. b) S. Horike, S. Shimomura, S. *Kitagawa*,*Soft* porous crystals. *Nat*. *Chem*. **2009**, *1*, 695-704.

[4] a) J. Perego, S. Bracco, M. Negroni, C. X. Bezuidenhout, G. Prando, P. Carretta, A. Comotti, P. Sozzani, Fast motion of molecular rotors in metal-organic framework struts at very low temperatures. *Nat. Chem.* **2020**, *12*, 845-851. b) J. Dong, V. Wee, S. B. Peh, D. Zhao, Molecular-Rotor-Driven Advanced Porous Materials. *Angew. Chem. Int. Ed.* **2021**, *60*, 16279-16292. c) A. Comotti, S. Bracco, P. Sozzani, Molecular Rotors Buit in Porous Materials. *Acc. Chem. Res.* **2016**, *49*, 1701-1710. d) C. S. Vogelsberg, M. A. Garcia-Garibay, Crystalline molecular machines: function, phase order, dimensionality, and composition. *Chem. Soc. Rev.* **2012**, *41*, 1892-1910. e) G. Prando, J. Perego, M. Negroni, M. Rocco, S. Bracco, A. Comotti, Molecular rotors in a metal-organic framework: muons on a hyper-fat carousel. *Nanolett.* **2020**, *20*, 7613-7618.

[5] a) J. Perego, C. X. Bezuidenhout, S. Bracco, G. Prando, L. Marchiò, M. Negroni, P. Carretta, P. Sozzani, A. Comotti, Cascade Dynamics of Multiple Molecular Rotors in a MOF: Benchmark Mobility at a Few Kelvins and Dynamics Control by CO_2. *J. Am. Chem. Soc.* **2021**, *143*, 13082-13090. b) J. Perego, C. X. Bezuidenhout, S. Bracco, S. Piva, G. Prando, C. Aloisi, P. Carretta, J. Kaleta, T. P. Le, P. Sozzani, A. Daolio, A. Comotti, Benchmark Dynamics of Dipolar Molecular Rotors in Fluorinated Metal-Organic Frameworks. *Angew. Chem. Int. Ed.* **2023**, *62*, e202215893.

[6] a) S. Horike, S. Shimomura, S. Kitagawa Soft Porous Crystals. *Nat. Chem.* 2009, *1*, 695-704. b) A. Schneemann, V. Bon, I. Schwedler, I. Senkovska, S. Kaskel, R. A. Fischer Flexible metal–organic frameworks. *Chem. Soc. Rev.*. **2014**, ***43***, 6062-6096.

[7] a) S. Krause, N. Hosono, S. Kitagawa, Chemistry of Soft Porous Crystals: Structural Dynamics and Gas Adsorption Properties. *Angew. Chem. Int. Ed.* **2020**, *59*, 15325-15341. b) C. Serre, F. Millange, C. Thouvenot, M. Noguès, G. Marsolier, D. Louër, G. Férey, Very Large Breathing Effect in the First Nanoporous Chromium(III)-Based Solids: MIL-53 or $Cr^{III}(OH)\cdot\{O_2C-C_6H_4-CO_2\}\cdot\{HO_2C-C_6H_4-CO_2H\}_x\cdot H_2O_y$. *J. Am. Chem. Soc.* **2002**, *124*, 13519-13526. c) E. G. Meekel, E. M. Schmidt, L. J. Cameron, A. D. Dharma, H. J. Windsor, S. G. Duyker, A. Minelli, T. Pope, G. O. Lepore, B. Slater, C. J. Kepert, A. L. Goodwin, *Science* **2023**, *379*, 357-361. d) V. I. Nikolayenko, D. C. Castell, D. Sensharma, M. Shivanna, L. Loots, K. A. Forrest, C. J. Solanilla-Salinas, K-I. Otake, S. Kitagawa, L. J. Barbour, B. Space, M. J. Zaworotko, Reversible transformations between the non-porous phases of a flexible coordination network enabled by transient porosity. *Nat. Chem.* **2023**, *15*, 542-549. e) J. Cao, W. Ma, K. Lyu, L. Zhuang, H. Cong, H. Deng, Twist and sliding dynamics between interpenetrated frameworks in Ti-MOF revealing high proton conductivity. *Chem. Sci.* **2020**, *11*, 3978-3985.

[8] a): M. Shivanna, Q. Y. Yang, A. Bajpai, E. Patyk-Kazmierczak, M. J. Zaworotko. A Dynamic and Multi-Responsive Porous Flexible Metal-Organic Material. *Nat. Comm.* **2018**, *9*, 3080 (1 of 7). b) J. Seo, R. Matsuda, H. Sakamoto, C. Bonneau, S. Kitagawa. A Pillared-Layer Coordination Polymer with a Rotatable Pillar Acting as a Molecular Gate for Guest Molecules. *J. Am. Chem. Soc.* **2009**, *131*, 12792–12800. c) I. Senkovska, V. Bon, L. Abylgazina, M. Mendt, J. Berger, G. Kieslich, P- Petkov, J. L. Fiorio, J.-O.Joswig, T. Heine, L. Schaper, C. Bachetzky, R. Schmid, R- A. Fischer, A. Pöppl, E. Brunner, S. Kaskel. Understanding MOF Flexibility: An Analysis Focused on Pillared Layer MOFs as a Model System. *Angew. Chem. Int. Ed.* **2023**, *62*, e202218076 (1 of 47).

[9] V. Guillerm, D. Kim, J. F. Eubank, R. Luebke, X. Liu, K. Adil, M. S. Lah, M. Eddaoudi, A supermolecular building approach or the design and construction of metal-organic frameworks. *Chem. Soc. Rev.* **2014**, *43*, 6141-6172.

[10] a) J. Harada, K. Ogawa, Invisible but Common Motion in Organic Crystals: A Pedal Motion in Stilbenes and Azobenzenes. *J. Am. Chem. Soc.* **2001**, *123*, 10884-10888. b) J. Harada, K. Ogawa, Pedal motion in crystals. *Chem. Soc. Rev.* **2009**, *38*, 2244–2252.

[11] a) A. Comotti, S. Bracco, P. Sozzani, Molecular Rotors Built in Porous Materials. *Acc. Chem. Res.* **2016**, *49*, 1701-1710. b) A. Comotti, S. Bracco, P. Valsesia, M. Beretta, P. Sozzani, Fast Molecular Rotor Dynamics Modulated by Guest Inclusion in a Highly Organized Nanoporous Organosilica. *Angew. Chem. Int. Ed.* **2010**, *49*, 1760-1764. c) S. Bracco, M. Beretta, A. Cattaneo, A. Comotti, A. Falqui, K. Zhao, C. Rogers, P. Sozzani, Dipolar Rotors Orderly Aligned in Mesoporous Fluorinated Organosilica Architectures. *Angew. Chem. Int. Ed.* **2015**, *54*, 4773-4777.

[12] K. Griffiths, N. R. Halcovitch, J. M. Griffin, Long-Term Solar Energy Storage under Ambient Conditions in a MOF-Based Solid−Solid Phase-Change Material. *Chem. Mater.* **2020**, *32*, 9925-9936.

[13] NMR Waudby, C. A.; Alfonso, I. An introduction to one- and two-dimensional lineshape analysis of chemically exchanging systems. *J. Magn. Res. Open* **2023**, *16-17*, 100102.

[14] R. Kubo, K. Tomita, A General Theory of Magnetic Resonance Absorption. *J. Phys. Soc. Jpn.* **1954**, *9*, 888-919.

[15] N. L. Owen, *International Rotation in Molecules*, Wiley-Interscience, **1974**; p. 157.

Entry for the Table of Contents

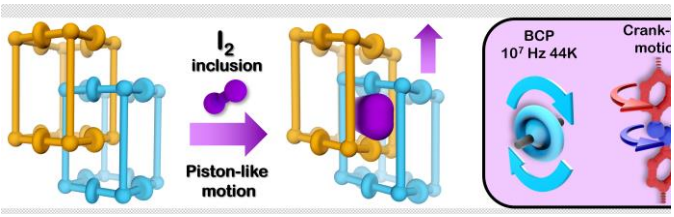

The flexible framework sliding governs the overall dynamical machinery. Moving elements, bicyclopentane, bipyridyls and azo groups, rotate with modulated dynamics in response to chemical stimuli such as I_2 vapors and pressurized CO_2 diffused into a pillared MOF.

Graphical Material

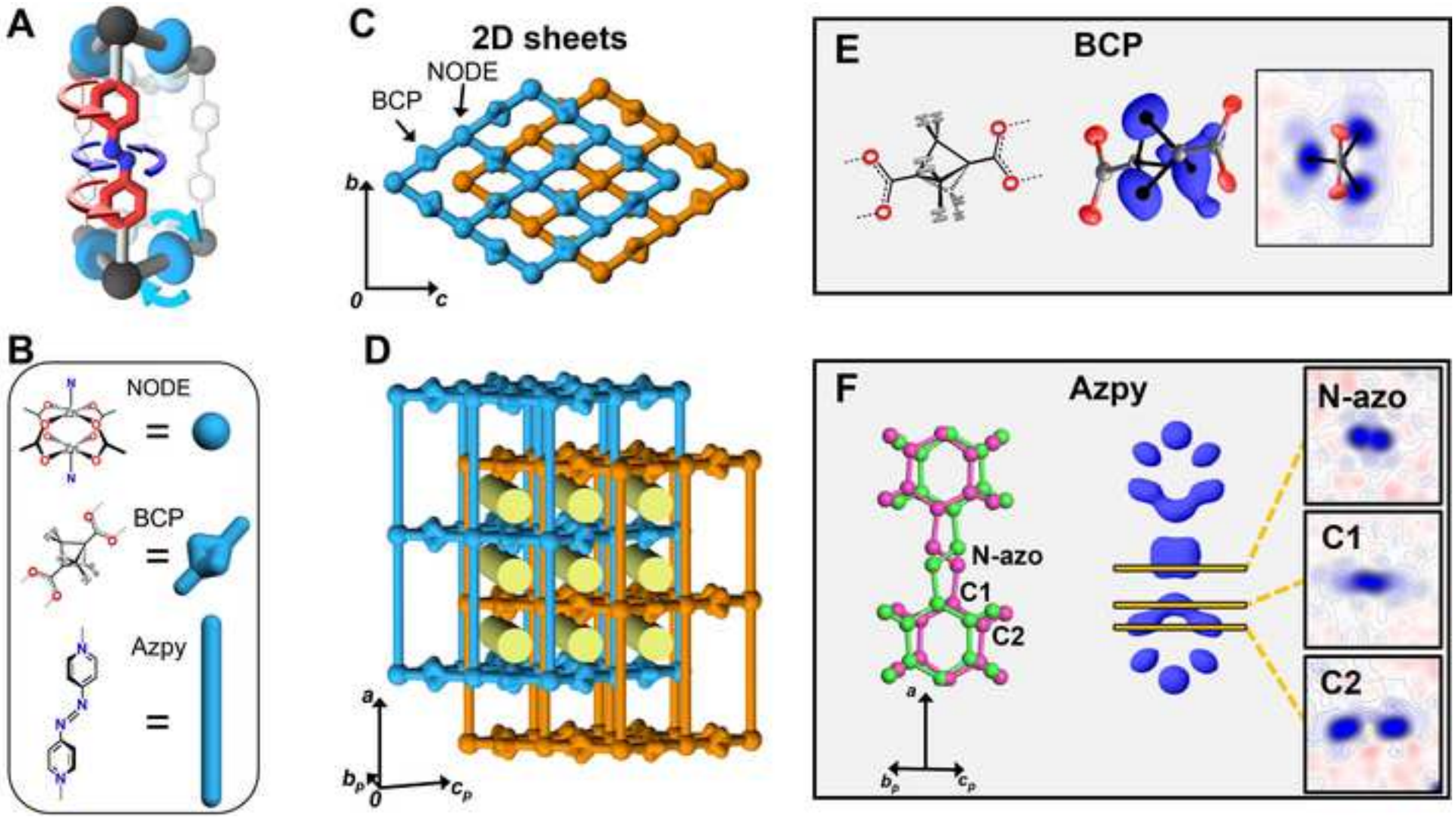

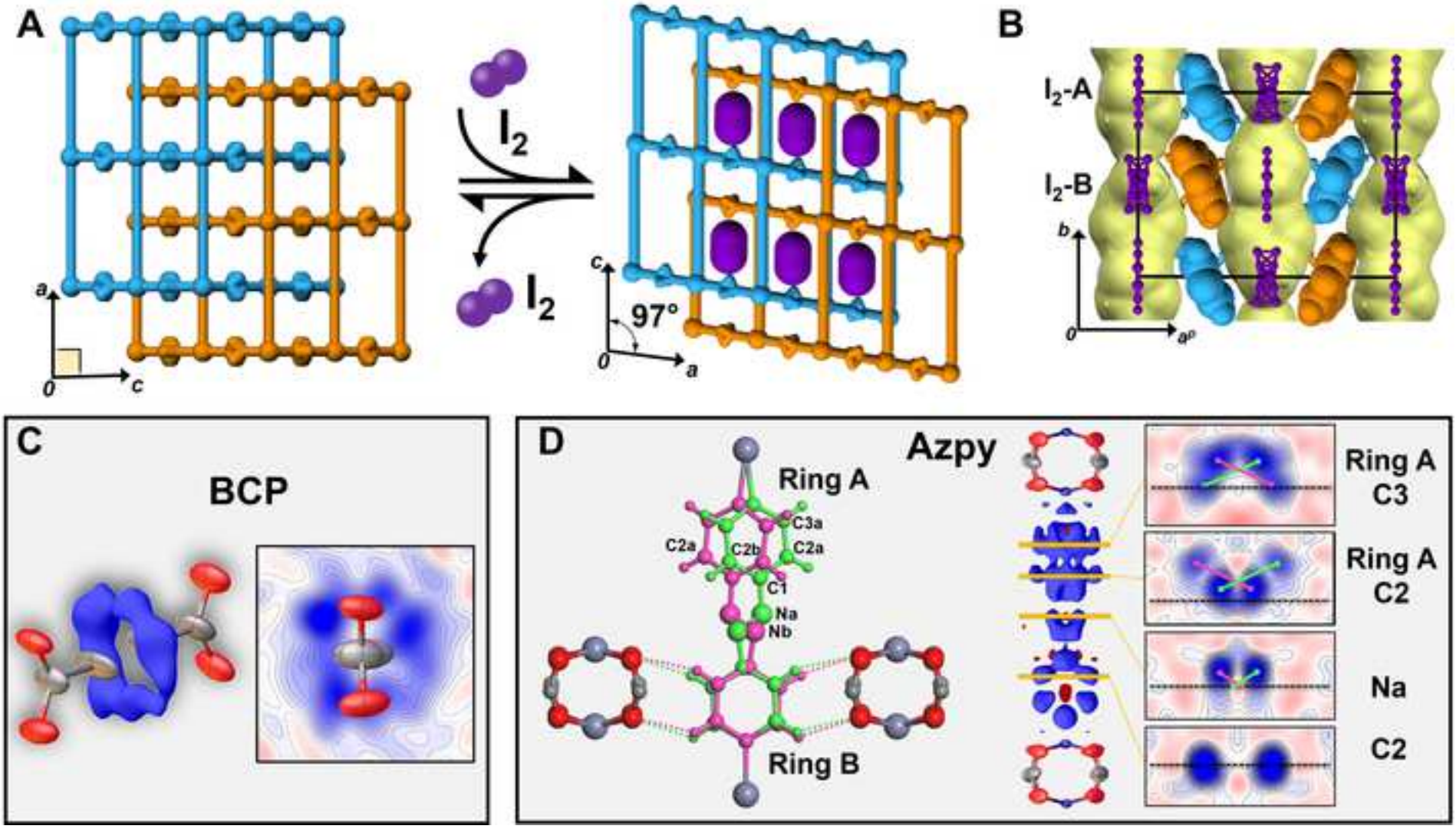
A
a
0
c
I2
I2
c
97°
0
a
B
I2-A
I2-B
b
0
a
C
BCP
D
Azpy
Ring A
C3a
C2a
C2b
C2a
C1
Na
Nb
Ring B
Ring A C3
Ring A C2
Na
C2

Graphical Material

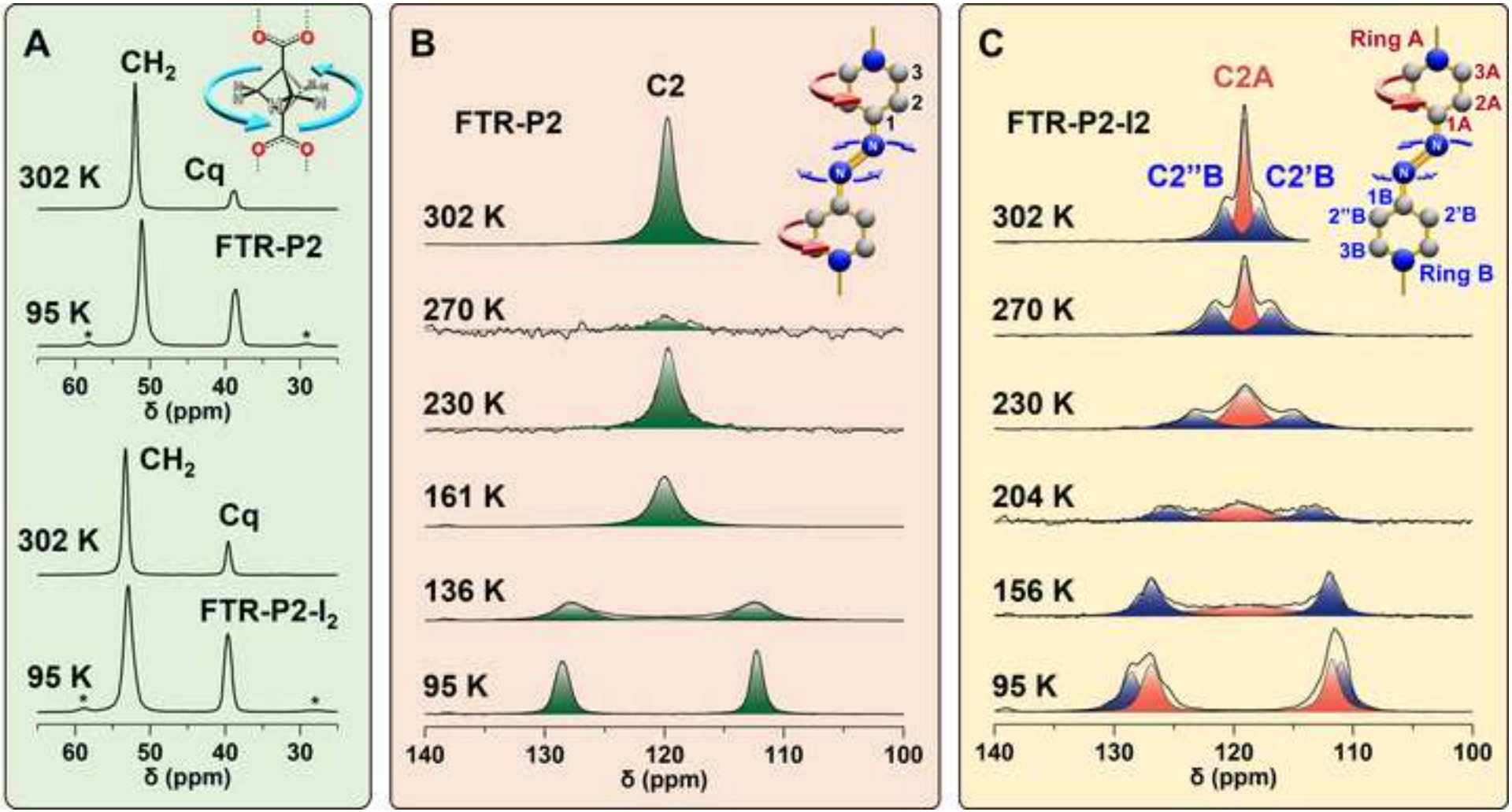

Graphical Material

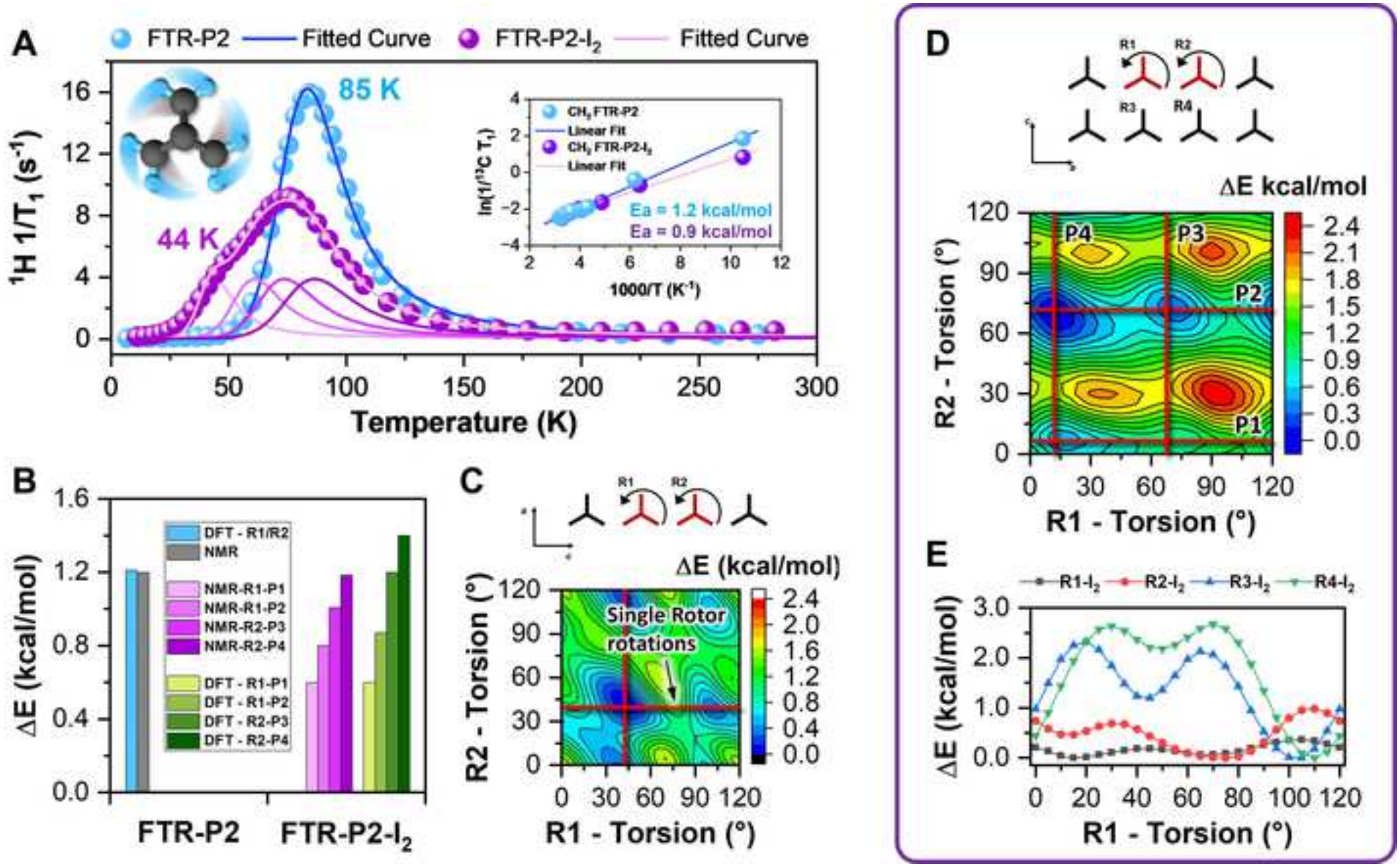

Graphical Material

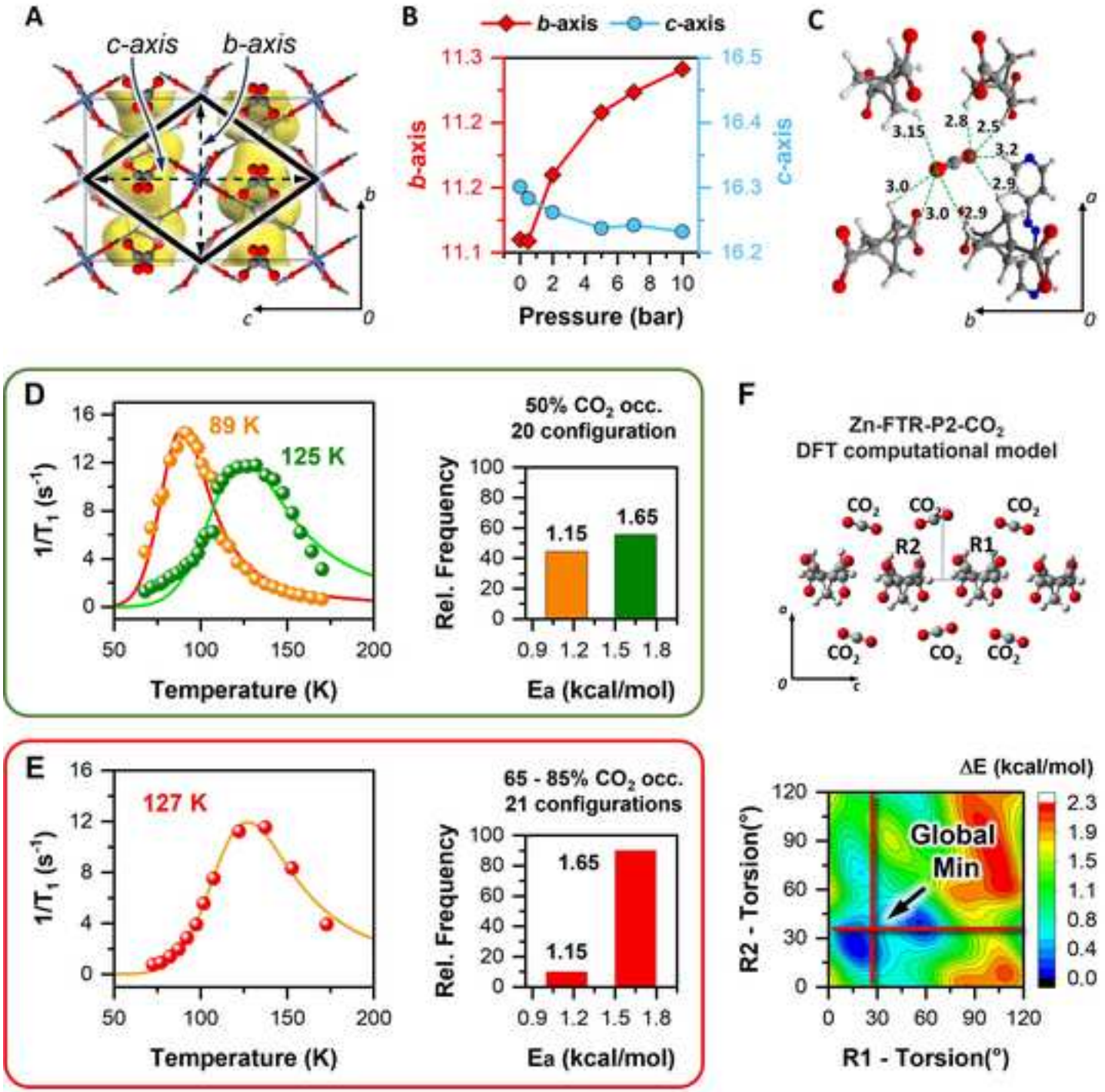

Graphical Material